High-Volume Single-Wafer Reactors for Silicon Epitaxy

ARTICLE *in* INDUSTRIAL & ENGINEERING CHEMISTRY RESEARCH · JANUARY 2002

Impact Factor: 2.59 · DOI: 10.1021/ie010412w

2 AUTHORS:

Srikanth Kommu
MEMC Electronic Materials, Inc.
11 PUBLICATIONS **98** CITATIONS
SEE PROFILE

Bamin Khomami
University of Tennessee
193 PUBLICATIONS **2,354** CITATIONS
SEE PROFILE

High-Volume Single-Wafer Reactors for Silicon Epitaxy

Srikanth Kommu[†,‡] and Bamin Khomami*[,†]

Department of Chemical Engineering and the Materials Research Laboratory, Washington University, St. Louis, Missouri 63130, and Epitaxial Silicon Technology, MEMC Electronic Materials, Inc., MZ 58, P.O. Box 8, 501 Pearl Drive, St. Peters, Missouri 63376

A detailed three-dimensional simulation model has been used to explore new designs and operating conditions that will lead to high-volume production of single-crystal silicon wafers in horizontal single-wafer reactors. As the $SiHCl_3-H_2$ system is a widely used precursor for epitaxial silicon deposition in industrial applications, we have chosen to focus our model development on this system. Specifically, we have examined cases where the wafer is placed in the entrance laminar region of a developing turbulent flow and, in a fully developed turbulent flow. It has been shown that a short height and high flow rate reactor is the best design for high-volume production of quality wafers with minimum material usage. In addition, it has been demonstrated that short height and high flow rate reactors are ideal for production of large diameter wafers that operate at low wafer temperatures.

I. Introduction

Chemical vapor deposition (CVD) is a process which uses chemically reactive gases to deposit thin solid films on a surface. The use of these thin solid films is widespread in many industries, such as microelectronics, magnetic materials, optical devices, automobiles, and ceramics. In the silicon-based semiconductor industry, CVD is used to deposit a wide variety of films, including polycrystalline silicon (polysilicon), epitaxial silicon, silicon oxides, and silicon nitrides. The advantage of the CVD process as compared to other deposition processes, such as evaporation, sputtering, and so forth, is that it is capable of producing thin films of a wide variety of materials with precisely defined and highly reproducible electrical, optical, chemical, and mechanical properties.[1]

The CVD process is a complex dynamical process involving simultaneous mass, momentum, and energy transport and complex chemical reactions. Hence, the quality of the films produced will be determined by the interactions of various transport processes and the chemical reactions in the CVD chamber, which in turn depend on process conditions such as flow rate, pressure, temperature, concentration of chemical species, reactor geometry, and so forth. The CVD film deposition techniques in the silicon industry need to fulfill general requirements, such as a high deposition rate, good thickness uniformity across a wafer, and minimum particulate generation. There is also a constant need for rapid production of wafers with tighter specifications, so there is a continuous need to improve process design and operation. Mathematical modeling and simulation provide an excellent means to make these improvements in process design and operation at a fast pace, and they also provide an excellent economic alternative to trial-and-error-based experimental techniques. The immediate benefits to be realized are fewer experiments, reduction in waste during experimentation, and the ability to deal with different reactive species and reactor geometries. In addition, simulation models can be used for optimization of the process conditions and reactor geometry as well as for design of new processes for high-volume wafer production.

II. Background

The CVD process is schematically shown in Figure 1. The sequence of steps that occur in a CVD process are described as follows:[2] (1) convective and diffusive transport of reactants from the reactor inlet to the wafer surface within the reactor chamber; (2) chemical reactions in the gas-phase leading to new reactive species and byproducts; (3) convective and diffusive transport of the reactants and reaction products from the homogeneous reactions to the wafer surface; (4) adsorption of these species on the wafer surface; (5) surface diffusion of adsorbed species over the surface; (6) heterogeneous surface reactions on the surface, leading to the formation of a solid film; (7) desorption of gaseous reaction products; and (8) convective and diffusive transport of reaction products to the outlet of the reactor. However, in recent years, the demand for wafers having a large diameter that meet highly tight specifications is on the rise. This has led to an increased interest in single-wafer reactors that can process high-quality wafers, one wafer at a time. Hence, in this study, we have focused our modeling efforts on horizontal single-wafer epitaxial reactors. In what follows, we will briefly summarize the most relevant prior work performed in this area to put into context our own efforts.

In the last two decades, the study of CVD deposition processes has burgeoned. The reason for this lies in the widespread use of CVD processes in production of wide variety of electronic materials. In most CVD processes, the initial mixture in the reactor is not allowed to reach equilibrium; as a result, most prior studies have taken into account the interactions between kinetics and transport in the design and optimization of CVD reactors.[1−14] Three-dimensional simulations in CVD reactors, where the deposition process is transport-limited,[3] as well as for systems such as silane, whose chemistry is well-understood,[4] have been successfully

* Corresponding author. Fax: 314-935-7211. E-mail: bam@poly1.che.wustl.edu.
[†] Washington University.
[‡] MEMC Electronic Materials, Inc.

10.1021/ie010412w CCC: $22.00
Published on Web 01/29/2002

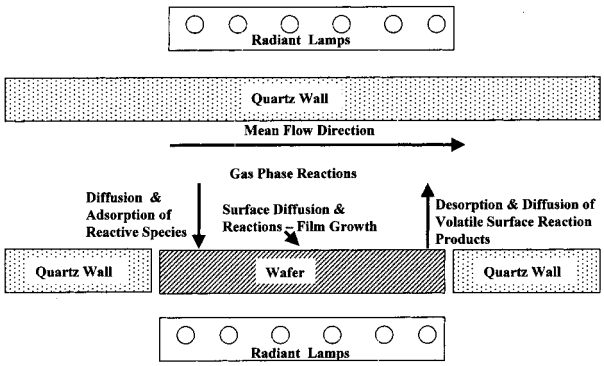

Figure 1. Schematic representation of a typical horizontal CVD reactor.

used to describe the reactor dynamics. For systems such as the $SiHCl_3-H_2$ mixture, whose chemistry of decomposition is not well understood, the success of three-dimensional modeling efforts in describing the dynamics of the reactor has also been recently demonstrated.[5] Prior studies[1−11] have successfully used the simulation models for determining the influence of different operating conditions on the reactor performance. Specifically, for horizontal reactor geometries using the $SiHCl_3-H_2$ system, Kommu et al.[5] have concluded that although it is not possible to exactly separate the influence of mass transfer and kinetics on the silicon deposition rate, the silicon deposition rate in the region near the leading edge of the wafer is more sensitive to the reaction kinetics, and the deposition rate at the trailing edge is more sensitive to the transport properties. This was rationalized by the fact that, near the leading edge, the mass-transfer boundary layer is thin; hence, the overall deposition rate is governed by the rate of reaction kinetics while, at the trailing edge, the ability to rapidly get the reactants to the wafer surface is the controlling factor due to the significant thickness of the mass-transfer boundary layer. Our aim in this study is to improve the deposition rate and thickness uniformity of epitaxial silicon in a single-wafer horizontal reactor. We have selected to study the $SiHCl_3-H_2$ mixture because this system is widely used for growing epitaxial films in industrial applications. Specifically, enhancement in the deposition rate will be realized by increasing the flow rate of the $SiHCl_3$ and H_2 gas mixture in such a way that the timescale for transport of species to the wafer (i.e., by reduction of the mass-transfer boundary layer thickness) is reduced as compared to the timescale for surface reaction, making epitaxial silicon deposition process almost entirely kinetically controlled. It should be noted that making the deposition process completely kinetically controlled is undesirable because the surface reaction rates are very sensitive to temperature variations.[5] Hence, if the wafer temperature is not maintained constant by the radiant lamps, significant variations in the epitaxial silicon thickness uniformity and wafer surface quality (i.e., slip lines, etc.) could result. However, because of the recent advances in the state-of-art rapid thermal processing (RTP) technology,[15] it is now possible to minimize the temperature nonuniformities across the wafer which justifies the consideration of making epitaxial silicon deposition more kinetically controlled.

To decrease the mass-transfer resistance in the deposition process, two approaches have been considered. The first approach relies on placement of the wafer in the entrance region of a developing turbulent flow, while the second approach relies on placement of the wafer in a fully developed turbulent flow. It should be noted that Santen et al.[16] have also used turbulent flow in rotating wafer CVD reactors to enhance the deposition rate. Finally, to make economic use of reactants, we have also considered the option of reducing the height of the reactor.

As briefly mentioned here and in our prior theoretical/experimental studies of single-wafer horizontal CVD reactor,[5] we have demonstrated that a detailed transport model in conjunction with proper deposition kinetics can quantitatively predict the deposition profile in single-wafer horizontal CVD reactor under laminar flow conditions. In this study, we have considered similar reactors as in the aforementioned study, with the exception the deposition process will be performed either in the entrance region of a developing channel flow or in a fully developed low Reynolds number turbulent channel. Considering the fact that both diffusive and convective transport of mass, momentum, and energy in the entrance region of a channel flow can be accurately predicted by the model proposed in our prior study as well as the fact that transport processes in fully developed low Reynolds number turbulent channel flow can be accurately modeled with the low Reynolds number $k - \epsilon$ model, the simulation results should provide quantitative predictions of the deposition profiles, hence obviating the need for a detailed experimental study.

The rest of this paper is organized as follows: section III describes the problem formulation, section IV describes the reaction kinetics used in this study, section V briefly discusses the computational details, section VI discusses the results of the simulation studies, and section VII provides a brief summary.

III. Problem Formulation

To develop a robust model that fully describes the transport and kinetics of chemical species in a CVD reactor, one needs to solve the appropriate set of governing equations under realistic boundary conditions, describing the gas flow, transport of energy and chemical species, and the chemical reactions in a CVD reactor. In such a model, the dependence of gas properties on gas composition and temperature as well as transport due to thermal diffusion should be considered. The governing equations used in the model have been arrived at using the following realistic assumptions for atmospheric pressure CVD: (1) the gases are considered to be ideal, obeying ideal gas law and Newton's law of viscosity; (2) the gas mixture is assumed to behave as a continuum (Knudsen number < 0.01); (3) the heat generated/consumed by chemical reactions is neglected, as the reactants are highly diluted; (4) heating due to viscous dissipation is neglected (Brinkman number < 0.01); (5) pressure variations in the energy equation are neglected, as the Mach numbers are very small; (6) the Dufour effect, which causes an energy flux in a gas mixture as a result of concentration gradients, is neglected; and (7) the eddy viscosity hypothesis is assumed, which essentially means that the turbulence is assumed to be characterized by only one length scale.

III.1. Governing Equations. As we are interested in determining the steady-state silicon deposition rate profiles on the wafer, the steady-state version of the governing equations has been used. However, as the

governing set of equations and boundary conditions contain several parameters, it is advantageous to write them in dimensionless form. Then, the effect of different dimensionless groups on the reactor performance can be studied.[5] To make the governing set of equations dimensionless, the following dimensionless variables are introduced:

$$\hat{U} = \frac{U}{V}; \quad \hat{T} = \frac{T}{T_{\text{wafer}}}; \quad \hat{w}_{\text{A}} = \frac{w_{\text{A}}}{w_{\text{A,in}}}; \quad \hat{P} = \frac{P_{\text{Ref}}}{\rho V^2};$$
$$\nabla = \nabla L; \quad \hat{\rho} = \frac{\rho}{\rho_{\text{Ref}}}; \quad \hat{\mu} = \frac{\mu}{\mu_{\text{Ref}}}; \quad \hat{\mu}_{\text{T}} = \frac{\mu_{\text{T}}}{\mu_{\text{T,Ref}}};$$
$$\hat{\mu}_{\text{eff,Ref}} = \frac{\mu_{\text{eff}}}{\mu_{\text{eff,Ref}}}; \quad \hat{\lambda} = \frac{\lambda}{\lambda_{\text{Ref}}}; \quad \hat{C}_p = \frac{C_p}{C_{p,\text{Ref}}};$$
$$\hat{D}_{\text{AB}} = \frac{D_{\text{AB}}}{D_{\text{AB,Ref}}}; \quad \hat{D}_{\text{A}}{}^{\text{T}} = \frac{D_{\text{A}}{}^{\text{T}}}{D_{\text{A,Ref}}^{\text{T}}} \quad (1)$$

where all of the reference properties are calculated at a reference temperature T_{Ref}, V is the characteristic velocity of the gas, $\mu_{\text{eff}} = \mu + \mu_{\text{T}}$ is the effective viscosity, and L is the characteristic reactor dimension (a summary of all of the symbols used is given in the Nomenclature section at the end of this paper). Using these dimensionless parameters, the governing equations take the following dimensionless forms:

(i) mass balance

$$\hat{\nabla}\cdot(\hat{\rho}\hat{U}) = 0 \quad (2)$$

(ii) chemical species balance

$$\hat{\nabla}\cdot(\hat{\rho}\hat{U}\hat{w}_{\text{A}}) = \frac{1}{Re}\hat{\nabla}\cdot\left(\left(\frac{\hat{\rho}\hat{D}_{\text{AB}}}{Sc} + \frac{\mu_{\text{T,Ref}}}{\mu_{\text{Ref}}}\frac{\hat{\mu}_{\text{T}}}{\sigma_{\text{A}}}\right)\hat{\nabla}\hat{w}_{\text{A}}\right) + \frac{1}{ReTd}\hat{\nabla}\cdot\left(\frac{\hat{D}_{\text{T}}}{\hat{T}}\hat{\nabla}\hat{T}\right) \quad (3)$$

where

$$Re = \frac{\rho_{\text{Ref}}VL}{\mu_{\text{Ref}}}; \quad Sc = \frac{\mu_{\text{Ref}}}{\rho_{\text{Ref}}D_{\text{Ref}}}; \quad Td = \frac{\mu_{\text{Ref}}w_{\text{A,in}}}{D_{\text{Ref}}{}^{\text{T}}} \quad (4)$$

(iii) momentum balance

$$\hat{\nabla}\cdot(\hat{\rho}\hat{U}\hat{U}) = \frac{1}{Re}\hat{\nabla}\cdot\left(-\frac{2}{3}\left(\left(\hat{\mu} + \frac{\mu_{\text{T,Ref}}}{\mu_{\text{Ref}}}\hat{\mu}_{\text{T}}\right)(\hat{\nabla}\cdot\hat{U})\cdot I + \frac{k_{\text{Ref}}\rho_{\text{Ref}}L}{\mu_{\text{Ref}}V}\hat{\rho}\hat{k}\right) + \left(\hat{\mu} + \frac{\mu_{\text{T,Ref}}}{\mu_{\text{Ref}}}\hat{\mu}_{\text{T}}\right)(\hat{\nabla}\cdot\hat{U} + (\hat{\nabla}\cdot\hat{U})^{\text{T}})\right) - \hat{\nabla}\hat{P} + \frac{Gr}{Re^2}\left(\frac{\hat{T} - \frac{1}{2}}{\left(\hat{T} - \frac{1}{2}\right)Ga + 1}\right)\hat{e}_z \quad (5)$$

where

$$Gr = \frac{g\rho_{\text{Ref}}^2L^3T_{\text{wafer}}}{\mu_{\text{Ref}}{}^2T_{\text{Ref}}}; \quad Pr = \frac{\mu_{\text{Ref}}C_{p,\text{Ref}}}{\lambda_{\text{Ref}}}; \quad Ga = \frac{T_{\text{wafer}}}{T_{\text{Ref}}} \quad (6)$$

(iv) energy balance

$$\hat{C}_p\hat{\nabla}\cdot(\hat{\rho}\hat{U}\hat{T}) = \frac{1}{Re}\hat{\nabla}\cdot\left(\frac{\hat{\rho}}{Pr} + \frac{\mu_{\text{T,Ref}}}{\mu_{\text{Ref}}}\frac{\hat{\mu}_{\text{T}}}{\sigma_{\text{H}}}\right)\hat{\nabla}\hat{T} \quad (7)$$

In general, thermal radiation should be considered when modeling high-temperature CVD reactors. However, inclusion of detailed radiation transport in the model will tremendously increase the CPU requirement of the simulations. Hence, in our earlier study of high-temperature CVD reactors,[5] an attempt was made to determine appropriate wall boundary condition for heat transfer that can quantitatively describe the temperature distribution on the reactor chamber surfaces. Specifically, by performing simulations with different temperature boundary conditions, we demonstrated that by using Robin-type boundary conditions at the reactor walls with an appropriate overall heat transfer coefficient and specifying the wafer temperature, the temperature profile in the reactor could be accurately determined. Hence, in this study, we have used the simpler approach of determining the temperature profile in the reactor. Specifically, an overall heat transfer coefficient of 50 W m^{-2} K^{-1} has been used.

To calculate the transport properties of the gas mixture in the aforesaid equations, the transport properties of the constituent species must be known. From the DIPPR database,[17] we have obtained the data on specific heat, viscosity, and thermal conductivity of relevant gas species as a function of temperature. In turn, we have used polynomial functions to fit these data as functions of temperature (see Appendix A). The binary diffusion coefficients (D_{AB}) and the thermal diffusion coefficients ($D_{\text{A}}{}^{\text{T}}$) were estimated using kinetic theory, and the variation of these properties with temperature have been determined (see Appendix B).

III.1.1. Turbulence Modeling. In order for the aforesaid governing equations to be closed, a constitutive equation for μ_{T} is required. This constitutive equation used in this study is based on a low Reynolds number turbulence model. Specifically, a modified version of the standard $k - \epsilon$ model that damps the eddy viscosity when the local turbulent Reynolds number is low has been used.[18,19] Hence, ϵ is defined such that it goes to zero at walls. The governing equations for k and ϵ are given as follows:

$$\hat{\nabla}\cdot(\hat{\rho}\hat{U}\hat{k}) = \frac{1}{Re}\hat{\nabla}\cdot\left(\hat{\mu} + \frac{\mu_{\text{T,Ref}}}{\mu_{\text{Ref}}}\frac{\hat{\mu}_{\text{T}}}{\sigma_{\text{k}}}\right)\hat{\nabla}k + \hat{P}_{\text{s}} + \hat{G}_{\text{b}} - \left(\frac{\epsilon_{\text{Ref}}L}{Vk_{\text{Ref}}}\right)\hat{\rho}\hat{\epsilon} - \hat{D} \quad (8)$$

$$\hat{\nabla}\cdot(\hat{\rho}\hat{U}\hat{\epsilon}) = \frac{1}{Re}\hat{\nabla}\cdot\left(\hat{\mu} + \frac{\mu_{\text{T,Ref}}}{\mu_{\text{Ref}}}\frac{\hat{\mu}_{\text{T}}}{\sigma_{\epsilon}}\right)\hat{\nabla}\hat{\epsilon} + C_1\frac{\epsilon_{\text{Ref}}\hat{\epsilon}}{k_{\text{Ref}}\hat{k}}\hat{P}_{\text{s}} - C_2f_2\left(\frac{\epsilon_{\text{Ref}}L}{Vk_{\text{Ref}}}\right)\frac{\hat{\rho}\hat{\epsilon}^2}{\hat{k}} + \hat{E} \quad (9)$$

where

$$\mu_{\text{T}} = C_\mu f_\mu\rho\frac{k^2}{\epsilon} \quad (10)$$

P_{s} is the shear production rate, defined as

$$\hat{P}_{\text{s}} = \left(\frac{\mu_{\text{eff,Ref}}V}{\rho_{\text{Ref}}Lk_{\text{Ref}}}\right)(\hat{\mu}_{\text{eff}}\hat{\nabla}\hat{U}\cdot(\hat{\nabla}\hat{U} + (\hat{\nabla}\hat{U})^{\text{T}})) - \frac{2}{3}\hat{\nabla}\cdot\hat{U}(\hat{\mu}_{\text{eff}}\hat{\nabla}\cdot\hat{U}) - \frac{2}{3}\hat{\nabla}\cdot\hat{U}(\hat{\rho}\hat{k}) \quad (11)$$

G_{b} is the production due to the body force, defined as

$$\hat{G}_b = -\left(\frac{\mu_{eff,Ref}\, g}{L}\right)\frac{\hat{\mu}_{eff}\,\hat{e}_z}{\hat{\rho}\sigma_p}\cdot\hat{\nabla}\hat{\rho} \tag{12}$$

and the additional terms are defined as

$$\hat{D} = \frac{2\hat{\mu}(\hat{\nabla}\hat{k}^{1/2})^2}{Re} \tag{13}$$

$$f_\mu = \exp\left(\frac{-3.4}{\left(1+\frac{R_T}{50}\right)}\right) \tag{14}$$

$$f_2 = 1 - 0.3\exp(-R_T{}^2) \tag{15}$$

$$\hat{E} = \left(\frac{2\mu_{Ref}\,\mu_{T,Ref}V}{\rho_{Ref}^2 L^3 \epsilon_{Ref}}\right)\frac{\hat{\mu}\hat{\mu}_T}{\hat{\rho}}(\hat{\nabla}\cdot\hat{\nabla}\hat{U})^2 \tag{16}$$

All of the constants in these equations are tabulated in Table 1.

III.2. Reactor Geometry. Figure 2 depicts a simplified version of a typical horizontal single-wafer CVD reactor used for silicon epitaxy. This reactor geometry has been used in all of the simulations reported in this study. The dimensions of the reactor are shown in the figure. In this idealized reactor, the gases are injected at room temperature (25 °C) through the inlet. The gases then pass through the quartz reactor chamber, which contains a silicon wafer placed at the bottom of the reactor and surrounded by a SiC ring. The wafer is heated radiatively by lamp arrays placed outside the quartz reactor chamber such that the wafer temperature is maintained constant (1400 K is a typical wafer temperature in epitaxial silicon reactors). The gases react in the chamber depositing the desired solid silicon film on the surface of the wafer. Finally, the reactant and product gases leave the reactor through the outlet, which is fixed at atmospheric pressure. The exterior surfaces of the reactor are cooled by air circulation.

III.3. Boundary Conditions. III.3.1. Walls. No slip boundary condition for the gas velocity is specified

$$\hat{U} = 0 \tag{17}$$

Robin-type boundary conditions are specified for the heat flux at the wall

$$n\cdot\nabla\hat{T} = \hat{h}(\hat{T} - \hat{T}_{Inf}) \tag{18}$$

Zero total mass flux for each of the chemical species is specified

$$n\cdot(\hat{j}_A{}^C + \hat{j}_A{}^T) = 0 \tag{19}$$

In the low Reynolds number $k-\epsilon$ model, the equations are integrated to the wall through the viscous sublayer adjacent to the walls. Hence, zero values of k and ϵ are used at the walls, that is,

$$\hat{k} = 0; \quad \hat{\epsilon} = 0 \tag{20}$$

III.3.2. Wafer. No slip boundary condition for the gas velocity is specified

$$\hat{U} = 0 \tag{21}$$

An isothermal boundary condition is used for the wafer surface. This is due the fact that the temperature of the wafer is maintained constant by the heat lamps

$$\hat{T} = \hat{T}_{wafer} \tag{22}$$

On the basis of the stoichiometry of an overall surface reaction leading to silicon deposition (i.e., $SiHCl_3(g) + H_2(g) \rightarrow Si(s) + 3HCl(g)$), the mass consumption and generation of each chemical species is taken into account as follows:

$$n\cdot(\hat{\rho}\hat{U}\hat{w}_A + \hat{j}_A{}^C + \hat{j}_A{}^T) = \hat{R}_{s,A} \tag{23}$$

The values of k and ϵ are specified to be equal to zero

$$\hat{k} = 0; \quad \hat{\epsilon} = 0 \tag{24}$$

III.3.3. Inlet. At the inlets, the velocity, temperature, and the composition of the gas mixture are specified, that is,

$$\hat{U} = \hat{U}_{in}; \quad \hat{T} = \hat{T}_{in}; \quad \hat{C}_A = \hat{C}_{A,in} \tag{25}$$

In general, it is not trivial to specify turbulence quantities at the inlet in absence of experimental data, so the inlet values of k and ϵ are specified based on mean flow characteristics. This is done by specifying a turbulence intensity and a dissipation length scale, that is,

$$\hat{k}_{in} = \left(\frac{V^2}{k_{Ref}}\right)1.5(i\hat{U}_{in})^2; \quad \hat{\epsilon}_{in} = \left(\frac{k_{Ref}^{0.5}}{\epsilon_{Ref}}\right)\frac{\hat{k}_{in}}{0.3D_l} \tag{26}$$

where i is the turbulence intensity (which is set to a value equal to 0.037)[20] and the dissipation length scale (D_l, which is reactor geometry dependent) is set equal to the characteristic length scale (L).

III.3.4. Outlet. At the outlet, atmospheric pressure is specified

$$P = P_{atm} \tag{27}$$

Zero flux boundary conditions are used for k, ϵ, temperature, and chemical species

$$n\cdot\hat{\nabla}\hat{T} = 0; \quad n\cdot\hat{\nabla}\hat{C}_A = 0; \quad n\cdot\hat{\nabla}\hat{k} = 0; \quad n\cdot\hat{\nabla}\hat{\epsilon} = 0 \tag{28}$$

Table 1. Values of the Constants in Low *Re* $k-\epsilon$ Turbulence Model

C_μ	0.09
C_1	1.44
C_2	1.92
σ_k	1.0
σ_ϵ	$\kappa^2/((c_2\text{-}c_1)c_\mu{}^{0.5})$
σ_H	0.9
σ_A	0.9
κ	0.4187

IV. Reaction Kinetics

An accurate kinetic model for $SiHCl_3$ decomposition needs to be coupled with the aforesaid transport model to predict silicon deposition rates as a function of different operating parameters. Kommu et al.[5] have demonstrated that a Langmuir−Hinshelwood-type surface kinetic mechanism quantitatively describes the kinetics of $SiHCl_3$ decomposition and the surface reaction kinetics leading to epitaxial silicon deposition. The details of the model are as follows. The reactants (i.e., $SiHCl_3$ molecules) are transported from the gas phase to the surface of the silicon wafer. $SiHCl_3$ molecules then attack the unoccupied reactive sites (i.e., the total

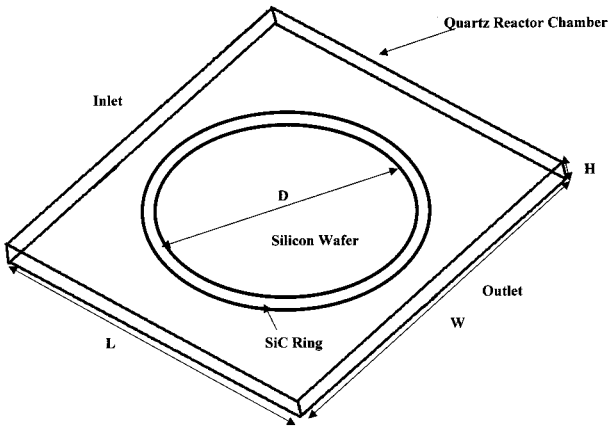

Figure 2. Schematic representation of simple rectangular single-wafer epitaxial silicon reactor: $L = 25$, $W = 25$, $H = 1.8$, and $D = 20$. All dimensions are in centimeters.

Table 2. Rate Constants at Different Temperatures

temperature (K)	K_{ad}(m/sec)	K_r(m/sec)
1373	1.00	3.83×10^{-3}
1398	1.00	4.23×10^{-3}
1423	1.00	4.63×10^{-3}

number of reactive sites are fixed) and decompose at a certain rate according to the following reaction:

$$SiHCl_3(g) \rightarrow SiCl_2^* + HCl(g) \tag{29}$$

Equation 29 is an adsorption reaction where $SiCl_2^*$ is the adsorbed species. The adsorbed $SiCl_2^*$ species is most likely bonded to the wafer surface with the two chlorine atoms pointing to the gas stream. Therefore, after adsorption, one ends up with a silicon surface covered with chlorine atoms. This adsorbed surface is then attacked by the hydrogen atoms to reduce $SiCl_2^*$ to Si and to release HCl gas according to the following reaction:

$$SiCl_2^* + H_2(g) \rightarrow Si(s) + 2HCl(g) \tag{30}$$

Hence, the overall silicon deposition rate is given by the following equation:

$$R_{Si} = \frac{K_{ad} C^s_{SiHCl_3}}{1 + \dfrac{K_{ad} C^s_{SiHCl_3}}{K_r C^s_{H_2}}} \tag{31}$$

where K_{ad} is the rate of adsorption reaction and K_r is the rate of desorption reaction. The values of K_{ad} and K_r have been determined by Kommu et al.[5] by performing a computationally assisted kinetic study and are tabulated as a function of temperature in Table 2.

V. Computational Details

The aforesaid governing equations coupled with the boundary conditions have been solved using an in-house developed Fortran code coupled with a commercially available software package CFX 4.1c from AEA Technology, Inc.,[20] which is based on the finite volume technique.[21]

Because of very large temperature gradients present near the silicon wafer in the reactor, the body force term in the momentum balance equation has not been approximated using the Boussinesq method. Instead, the density term in the buoyancy term is written as

$$\rho = \rho_0 + (\rho - \rho_0) \tag{32}$$

where ρ_0 is a reference density calculated at the reference gas temperature and the term $\rho_0 g$ is absorbed into the pressure gradient term of eq 8. The numerical solutions are assumed to be converged when the error in the continuity equation falls below 0.1% of the total mass flow rate entering the system, as well as when the residuals of all other variables such as velocity, pressure, chemical species, k, ϵ, and enthalpy fall bellow 10^{-8}.

VI. Results and Discussion

VI.1. Kinetics of Single-Crystal Silicon Growth. In the absence of mass-transfer resistance, only the intrinsic surface reaction kinetics will determine the silicon deposition rate at a fixed wafer temperature and a given gas composition. Therefore, making use of eq 31, it is possible to determine the deposition rate as a function of the initial concentration of the $SiHCl_3-H_2$ mixture in the absence of mass-transfer resistance for the three constant wafer temperatures at which the rate constants have been determined by Kommu et al.[5] Figure 3 shows these intrinsic deposition rates as a function of the initial concentration of $SiHCl_3$. Clearly, the silicon deposition rate increases with the increasing concentration of $SiHCl_3$ but decreases beyond an initial $SiHCl_3$ mass fraction of 0.82. This is due to the fact that the Langmuir−Hinshelwood kinetics are a two-step reaction (i.e., the adsorption reaction rate is proportional to the $SiHCl_3$ concentration and the desorption reaction rate is proportional to the H_2 concentration). As $w_{SiHCl_3,in} = 1 - w_{H_2,in}$, there exists a critical concentration of the $SiHCl_3-H_2$ mixture at which the deposition rate is a maximum. As shown by Figure 3, the maximum deposition rate is, in fact, attained at an initial $SiHCl_3$ mass fraction of 0.82 and is of the order of 20 micron/min at all three wafer temperatures. However, under typical operating conditions of 1 atm, a wafer temperature of 1400 K, and an initial $SiHCl_3$ mass fraction of 0.8, deposition rates in the commercial reactors are of the order of 4 micron/min. This clearly shows that the epitaxial silicon deposition rate can be increased 5-fold in typical commercial CVD reactors. However, one must ensure that the deposited layer forms a single silicon crystal. To estimate the upper limit of deposition rate for single-crystal silicon deposition, we have used the experimental results by Bloem[22] that show single-crystal growth occurs under atmospheric pressure conditions when the deposition rate satisfies the inequality given here

$$G < 4 \times 10^{19} \exp(-57876/T) \tag{33}$$

Using this criterion, it can be shown that, at typical operating conditions of 1 atm and a wafer temperature of 1400 K, a single-crystal deposition rate of the order of 40 micron/min is possible. Figure 3 clearly demonstrates that the maximum deposition rate that can be attained in typical CVD reactors is of the order of 20 micron/min, which is well below the upper limit for single-crystal silicon growth. This clearly shows that the rate of production of single-crystal silicon in typical commercial CVD reactors can be increased 5-fold. In

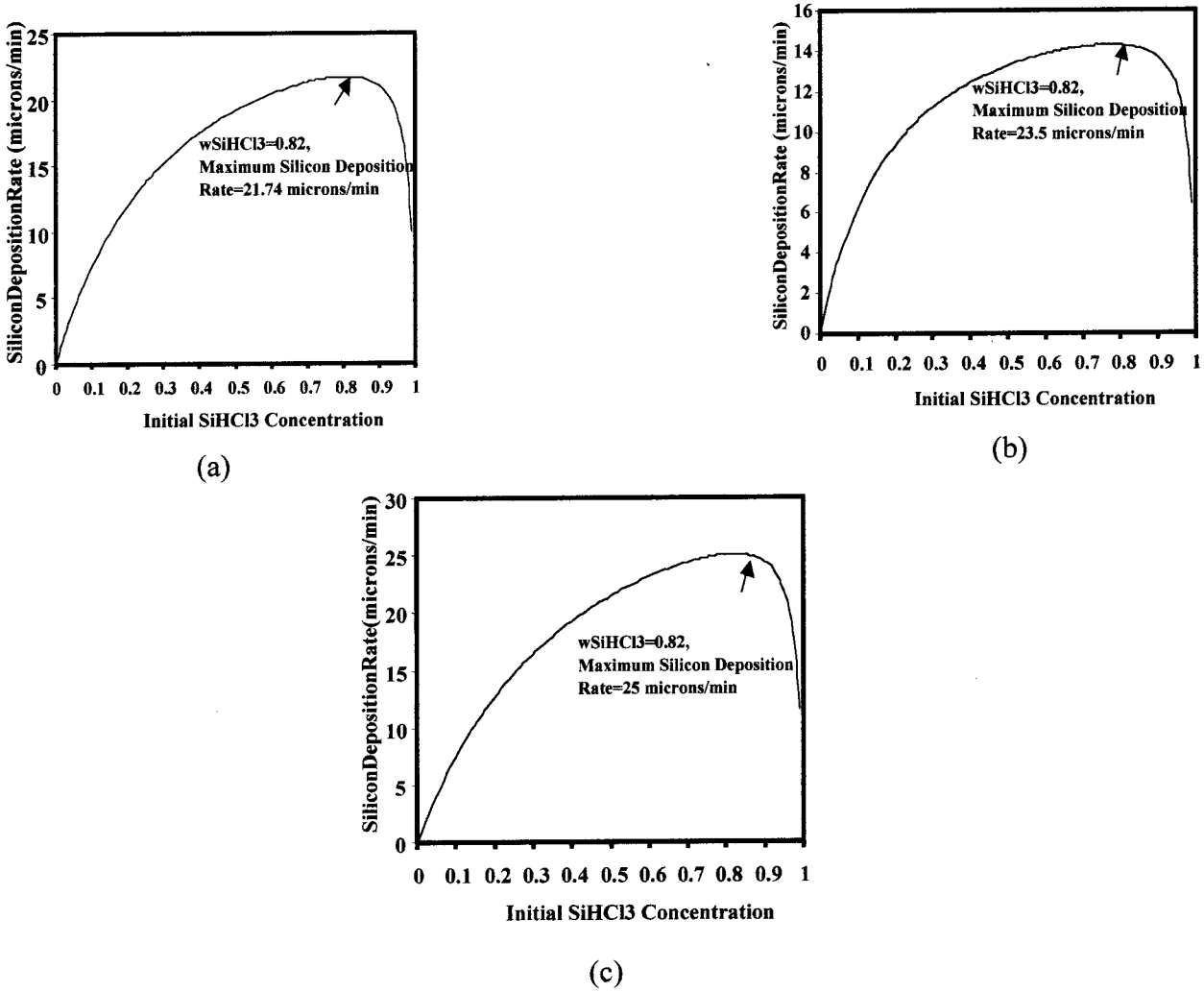

Figure 3. Silicon deposition rate as a function of initial concentration of a $SiHCl_3-H_2$ gas mixture under completely kinetically controlled conditions at three different T_{wafer}: (a) 1373 K, (b) 1398 K, and (c) 1423 K.

what follows, two reactor design strategies for high-volume production of single-crystal epitaxial silicon will be discussed.

VI.2. Laminar Flow Regime. Figure 4 shows the computational domain. To resolve the boundary layer near the reactor walls and the wafer surface, the mesh is highly refined along the *Y* direction. The total number of finite volumes in the domain is equal to 317 400, and the typical CPU time for numerical convergence of the coupled overall mass, momentum, and energy equations is on the order of 60 min on a Silicon Graphics Octane workstation. Using this solution as an initial guess, and coupling the chemical species balance equations with the mass, momentum, and energy balance equations leads to a converged numerical solution, again, on the order of 60 min. To ensure that the solutions generated with the mesh shown in Figure 4 are accurate, selected computations using a much more refined mesh consisting of 600 000 cells were performed. Overall, we did not find a significant difference between the results from the two meshes (i.e., the maximum difference between the computed results is less than 2%). Hence, the results shown below are based on the mesh shown in Figure 4.

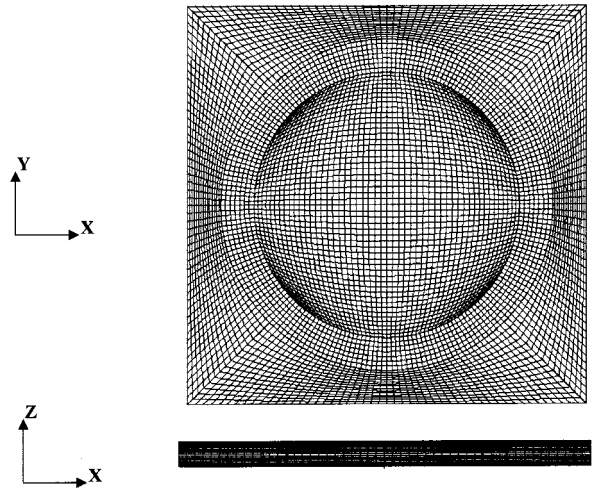

Figure 4. Domain discretization for the rectangular reactor geometry. The total number of finite volume cells equals 317 400. (Top) Projection of the mesh along the X−Y midplane. (Bottom) Projection of the mesh along the *X*−*Z* midplane.

To clearly demonstrate the relative importance of kinetic and mass-transfer resistances, the silicon deposition rates are made dimensionless with respect to the maximum possible deposition rate (i.e., silicon deposition rate in absence of mass-transfer resistance) at the given wafer temperature and an initial composition of the $SiHCl_3-H_2$ gas mixture. The maximum possible deposition rate is determined by the intrinsic surface

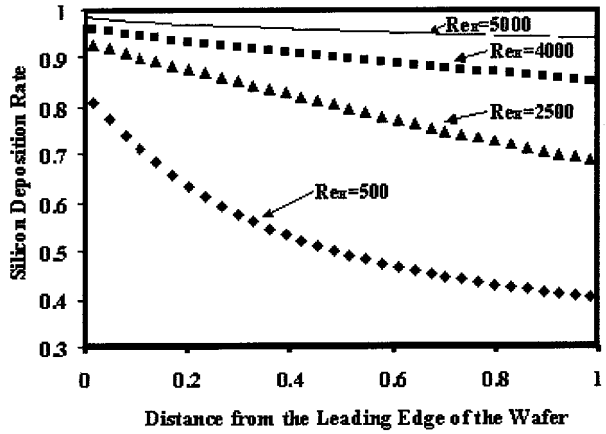

Figure 5. Dimensionless silicon deposition rate profile in the mean flow direction along the dimensionless centerline of the wafer (i.e., ratio of the distance from the leading edge of the wafer to wafer diameter (200 mm)) as a function of Re_H: $T_{wafer} = 1423$ K, $w_{SiHCl_3,in} = 0.82$.

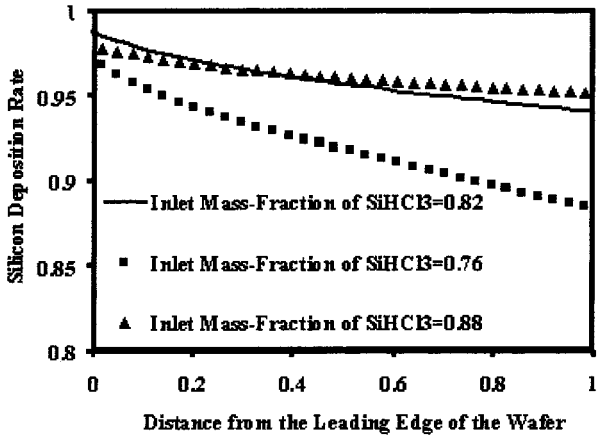

Figure 6. Dimensionless silicon deposition rate profile in the flow direction along the dimensionless centerline of the wafer (i.e., ratio of the distance from the leading edge of the wafer to wafer diameter (200 mm)) as a function of $w_{SiHCl_3,in}$: $Re_H = 5000$, $V_{in} = 30$ m/sec, $T_{wafer} = 1423$ K.

kinetics (see eq 31). Hence, the dimensionless deposition rate, G_d, provides a clear measure of the role of mass-transfer resistance in the deposition process. Specifically, if $G_d = 1$, the deposition process is completely kinetically controlled, and $G_d < 1$ implies that the reduction in deposition rate is due to the presence of mass-transfer resistance. Clearly, there are other methods for characterizing the relative importance of kinetics and mass-transfer resistance, such as the use of Damkohler number or a Thiele modulus. However, these dimensionless groups also convey the same information.

In Figure 5, the effect of varying the Reynolds number defined based on the reactor height as the reference length Re_H on G_d along the centerline of the wafer in the mean flow direction is illustrated for a wafer temperature of 1423 K and an initial $SiHCl_3$ mass fraction of 0.82. Clearly, some of the simulations have been performed at relatively high Re_H, which may suggest that the flow is turbulent. Indeed, the fully developed flow would be turbulent for the higher Re_H number flows. However, the wafer is placed in the entrance section of the reactor where the boundary layers are laminar (i.e., Re_x, the Reynolds number based on the reactor length is less than 3.2×10^5).[23] However, to ensure that the flow is indeed laminar, random disturbances are added to the steady-state solution of the velocity field at every node in the numerical domain, and using this field as an initial solution, transient simulations with different temporal and spatial discretizations have been performed. By monitoring the disturbance fluctuations, we have ensured that the disturbances die out over the entire range of operating conditions, indicating that the flow in the entrance region is indeed laminar.

Figure 5 clearly demonstrates that the silicon deposition rate increases with increasing Re_H. This is due to the fact that the mass-transfer boundary layer thickness becomes thin as a result of which the rate of mass flux of $SiHCl_3$ to the wafer surface is increased. Moreover, an increase in Re_H has a pronounced effect on the deposition rate profile. Specifically, as Re_H is increased, the variation in the deposition rate from the leading edge to the trailing edge of the wafer is decreased. This is due to the fact that as Re_H is increased, the mass-transfer resistance becomes reduced in comparison to the kinetic resistance, and under nearly kinetic controlled conditions, the wafer temperature uniformity dictates the thickness uniformity of the deposition rate profile. Under complete kinetic controlled conditions, if the wafer temperature is uniform, the thickness nonuniformity will be zero. Current industrial regulations dictate that the thickness nonuniformity across the wafer must be within 2%. Figure 5 clearly demonstrates that, for the reactor geometry considered in Figure 4, at $Re_H = 5000$, the thickness nonuniformity across the silicon wafer is close to meeting the industrial requirement. So, operating at a $Re_H = 5000$ leads to high deposition rates as well as to excellent thickness uniformity without a need for wafer rotation and flow adjustment across the reactor inlet.[5] In addition, high Re_H flows also lead to the elimination of buoyancy-driven recirculations, which are undesirable under normal reactor operating conditions as they are considered to be mainly responsible for particle contamination of wafers.[5]

For $Re_H = 5000$ (i.e., for a fixed inlet volumetric flow rate in a given reactor geometry using the $SiHCl_3-H_2$ gas mixture), the other means of increasing deposition rate is to consider varying the wafer temperature and the initial mass fraction of $SiHCl_3$. In Figure 6, the effect of varying the initial gas composition on silicon deposition rates along the centerline of the wafer in the mean flow direction is illustrated for $Re_H = 5000$ and a wafer temperature of 1423 K. Figure 6 shows that the silicon deposition rate increases with an increase in initial $SiHCl_3$ mass fraction up to $w_{SiHCl_3,in} = 0.82$, in accordance with the discussion in section VI.1. Figure 6 also shows an interesting phenomena in the deposition rate profiles for the following initial $SiHCl_3$ mass fractions, $w_{SiHCl_3,in} = 0.82$ and 0.88. Specifically, it shows that, up to a dimensionless distance of about 0.5 from the leading edge of the wafer, the silicon deposition rate for $w_{SiHCl_3,in} = 0.88$ is lower than the silicon deposition rate for $w_{SiHCl_3,in} = 0.82$ but that beyond this distance, the deposition rate is higher. This can be rationalized by considering the fact that the surface concentration of $SiHCl_3$ decreases along the wafer surface in the mean flow direction because of the increase in the mass-transfer boundary layer thickness and because of the consumption of $SiHCl_3$ at the wafer surface. Hence, in the $w_{SiHCl_3,in} = 0.88$ profile case, the wafer surface

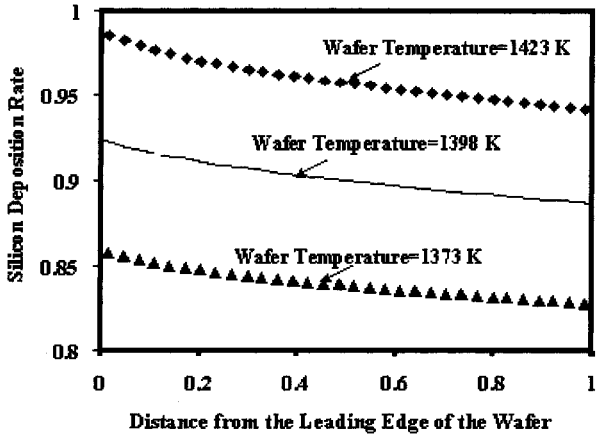

Figure 7. Dimensionless silicon deposition rate profile in the flow direction along the dimensionless centerline of the wafer (i.e., ratio of the distance from the leading edge of the wafer to wafer diameter (200 mm)) as a function of T_{wafer}: $Re_H = 5000$, $V_{in} = 30$ m/sec, $w_{SiHCl_3,in} = 0.82$.

concentration of $SiHCl_3$ ($w_{SiHCl_3,wafer}$) decreased along the mean flow direction. This, in turn, leads to an increase in the silicon deposition rate (i.e., the decrease in the surface concentration between 0.88 and 0.82 leads to an increase in deposition rate in accordance with the Langmuir−Hinshelwood kinetics, as shown in Figure 3). However, the increase is not very significant because $w_{H_2,wafer}$ is also reduced. It should be noted that, under these conditions, $w_{H_2,wafer} = 1 - (w_{SiHCl_3,wafer} + w_{HCl,wafer})$. This clearly demonstrates that, for determining an optimum composition for operating the reactor, one has to take into account transport effects.

In Figure 7, the effect of varying the wafer temperature on silicon deposition rates along the centerline of the wafer in the mean flow direction for $Re_H = 5000$ and an initial $SiHCl_3$ mass fraction of 0.82 is illustrated. Figure 7 shows that the silicon deposition rate increases with an increase in the wafer temperature. However, currently, a wafer temperature of 1423 K is close to the maximum temperature of a wafer in a commercial reactor such that there are minimum temperature variations across the wafer. Hence, we have not examined high-temperature cases.

Figure 8 shows the dimensionless mass fraction of $SiHCl_3$ as a function of dimensionless height above the center of the wafer for all the Re_H considered. As expected, the mass-transfer boundary layer thickness decreases with increasing Re_H. However, at $Re_H = 5000$, the mass-transfer boundary layer thickness is about 20% of the reactor height. Hence, it is possible to consider reducing the reactor height without significantly affecting the deposition rate and deposition profile while minimizing the amount of nonreacted feed exiting the reactor. Figure 8 also shows that the temperature boundary layer thickness decreases with increasing Re_H. Therefore, reducing the reactor height will not lead to issues such as over-heating of the top quartz reactor wall.

Table 3 shows the percentage conversion of mass leading to epitaxial silicon deposition as compared to the total mass flow rate entering the reactor for different Re_H for a wafer temperature = 1423 K and $w_{SiHCl_3} = 0.82$. It is clearly seen that the percentage of mass converted decreases with an increase in Re_H. Specifically, for $Re_H = 5000$, the percentage conversion is very low. However, operating the reactor at $Re_H = 5000$

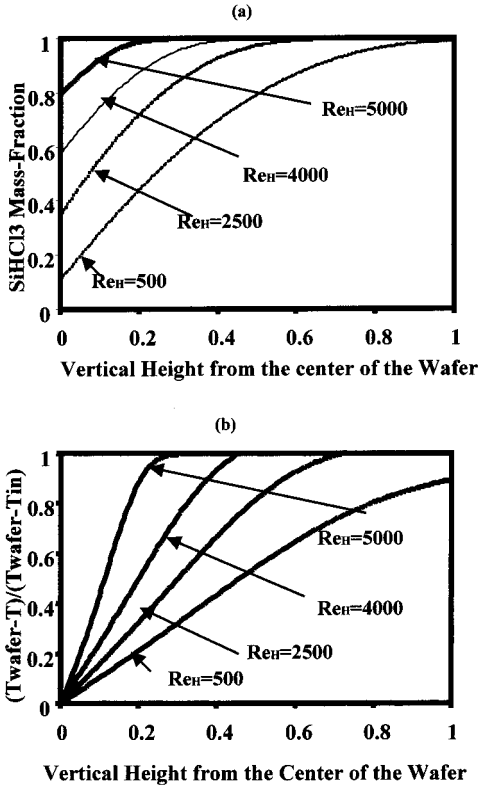

Figure 8. Effect of Re_H on the scaled (a) mass fraction profile of $SiHCl_3$ and (b) temperature profile, along the dimensionless vertical height between the center of the wafer and the top reactor wall: $T_{wafer} = 1423$ K, $w_{SiHCl_3,in} = 0.82$.

Table 3. Percentage of Mass Conversion for Different Re_H

Re_H	% mass conversion	Re_H	% mass conversion
500	1.290	4000	0.250
2500	0.580	5000	0.152

results in high deposition rate as well as excellent epitaxial silicon thickness uniformity. Specifically, these analyses have shown that, for a $SiHC_3-H_2$ precursor in the reactor geometry considered, the optimum conditions for maximizing silicon deposition rate and minimizing silicon thickness nonuniformity are $Re_H = 5000$, $T_{wafer} = 1423$ K, and $w_{SiHCl_3} = 0.82-0.9$. However, to address the low mass conversion issue, other strategies should be explored. One strategy is to explore the possibility of recycling the reactant gases, which involves purifying the gas-mixture exiting the reactor and feeding the purified gases back into the reactor. Another strategy involves making modifications to the reactor geometry. The following section briefly considers the latter design modification strategy.

Following the strategy of reducing the reactor height for the same inlet gas velocity, we have determined that if the reactor height is less than approximately $0.5H$ (H = height of the original reactor; see Figure 2), the characteristic velocity of the gas mixture will begin to slightly change. Figure 9 shows the comparison between silicon deposition rates in original laminar reactor and in the reduced height ($0.5H$) laminar reactor. This figure clearly demonstrates that, under these conditions, slightly better deposition rates can be attained, with the added benefit of minimizing the amount of nonreacted feed exiting the reactor (see Table 4 for comparison of percentages of mass conversion). However, a further decrease in reactor height leads to the case where the

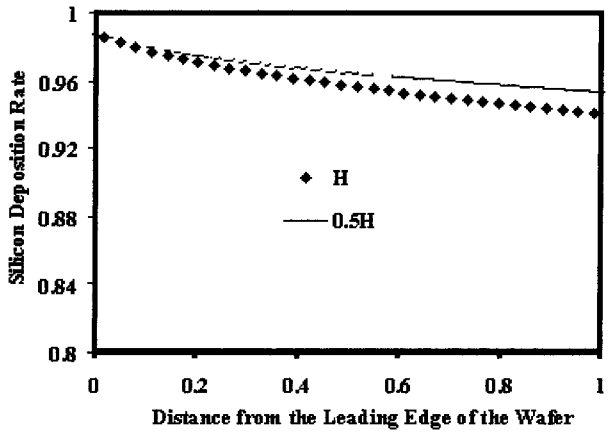

Figure 9. Effect of reactor height on dimensionless silicon deposition rate profile in the flow direction along the centerline of the wafer for the same inlet velocity of a $SiHCl_3-H_2$ gas mixture: $Re_H = 5000$, $V_{in} = 30$ m/sec, $Re_H(H = 0.5H) = 2500$.

Table 4. Percentage of Mass Conversion for Different Reactor Heights ($Re_H = 5000$)

height of the reactor	% mass conversion
H	0.152
$0.5H$	0.306
$0.1H$	1.55

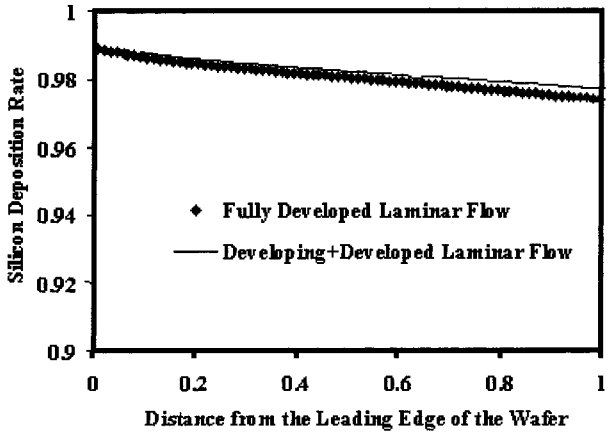

Figure 10. Dimensionless silicon deposition rate profile in the flow direction along the centerline of the wafer for a reactor of height $0.1H$: $V_{in} = 30$ m/sec, $Re_H = 500$, $T_{wafer} = 1423$ K, and $w_{SiHCl_3,in} = 0.82$.

wafer is no longer in the entrance region of a developing flow. In fact, the wafer is placed in a fully developed laminar flow. This is due to the fact that, for a fixed wafer diameter of 200 mm, reducing the reactor height while maintaining the same mean velocity leads to a very small entrance length and a reduction in Re_H. Figure 10 shows the deposition rate profile when the height of the reactor is reduced to $0.1H$ and the same initial velocity of the gas mixture is maintained. In this figure, the deposition rates for the case where the wafer is placed in a fully developed laminar flow and the case where the wafer is placed very close to the inlet such that a small section of the wafer is in the entrance region of the developing laminar flow in the reactor are shown. Clearly, the deposition rate magnitude and uniformity for the wafer placed in the entrance region are slightly better than that for the wafer placed in the fully developed laminar flow, but for all practical purposes, this difference is insignificant. These analyses clearly demonstrate that excellent thickness uniformity and high deposition rate can be attained when the reactor height is significantly reduced. Theoretically, the height of the reactor can be further reduced, but there may be mechanical constraints involved in placing the wafer in the reactor, so it was decided that $0.1H$, which corresponds to about 2 mm, is the smallest height considered in this study. Table 4 clearly shows that, for the reactor with height $= 0.1H$, the material usage is minimized and extremely high deposition rates and excellent thickness uniformity are attained.

In recent years, the demand for wafers having a large diameter that meet highly tight specifications is on the rise. However, maintaining a large diameter wafer at a constant temperature is a concern, particularly at temperatures of about 1400 K. As temperature differences may lead to wafer quality issues such as slip lines, it is conceived that these large diameter wafer reactors will be operated at lower temperatures. However, at low temperatures, the deposition rates will be low, and in the presence of mass-transfer resistance, the yield from these reactors will be extremely low, making the short height high flow rate reactors a very attractive option for large diameter wafer reactors. For example, films with excellent thickness uniformity can be attained at 1373 K with deposition rates as high as 20 micron/min at 1373 K in a high flow rate reactors with the height $0.1H$.

VII.2. Fully Developed Turbulent Flow. Simulations have been performed in order to determine the shape of the deposition rate profile when the wafer is placed in a fully developed turbulent flow field. The idea being that, in a turbulent flow, there will be enhanced mass transfer to the wafer surface due to reduction in the mass-transfer boundary layer thickness. The reactor domain used for turbulent flow simulations has the same width and height used for the laminar flow simulations but has an elongated reactor length (50 times original reactor length) in order to satisfy the condition that the Re_x is large enough for the flow to become turbulent. The turbulent flow simulations have been performed using the low Reynolds number $k - \epsilon$ model (see eqs 8−16). The same mesh discretization used for Laminar flow simulations (Figure 4) is used for turbulent flow simulations in the region around the wafer, to have a consistent comparison of results as well as to resolve the thin viscous sublayers present close to the reactor walls. The total number of finite volumes in the domain is equal to 450 800, and the difference in the number of finite volumes between this mesh and the mesh used for the laminar case is due to the increased length of the reactor here. Typical CPU time for numerical convergence of the coupled overall mass, momentum, turbulence, and energy equations is on the order of 120 min on a Silicon Graphics Octane workstation. Using this solution as an initial guess, and coupling the chemical species balance equations with the mass, momentum, turbulence, and energy balance equations leads to a converged numerical solution on the order of 360 min. To verify the accuracy of our simulation results, the computed velocity profiles at $Re_H = 5000$ have been compared with the universal velocity-distribution law[23] (see Figure 11). The excellent comparison between the profiles clearly demonstrates the accuracy of the computed solution. To further ensure that the solutions generated with the 450 800 cell mesh are accurate, selected computations using a much more refined mesh consisting of 600 000 cells were performed.

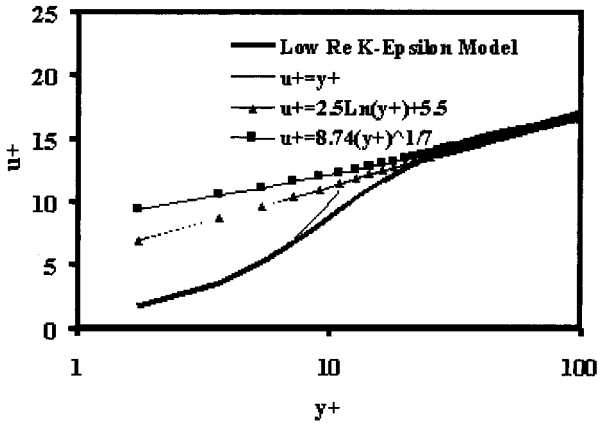

Figure 11. Comparison of velocity profile along the line between the center of the wafer and the midway point between the center of the wafer and reactor top wall with the universal velocity distribution law.

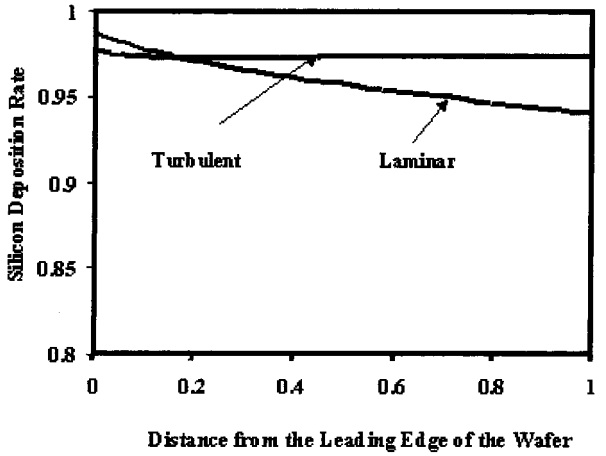

Figure 12. Comparison of dimensionless silicon deposition rate profiles in the flow direction along the centerline of the wafer when the wafer is placed in the developing laminar regime of a turbulent flow and when the wafer is placed in a fully developed turbulent flow: $Re_H = 5000$ ($H = H$), $V_{in} = 30$ m/sec, $T_{wafer} = 1423$ K, and $w_{SiHCl_3,in} = 0.82$.

Overall, we did not find a significant difference between the results from the two meshes (i.e., the maximum difference between the computed results is less than 2%). Hence, the results shown below are based on the 450 800 cell mesh.

Figure 12 shows a comparison of the dimensionless deposition rate profiles, G_d, when the wafer is placed in the entrance region of a developing turbulent flow and when the wafer is placed in the fully developed turbulent flow at $Re_H = 5000$. Clearly, the silicon deposition rate uniformity when the wafer is placed in the fully developed turbulent flow field is much better than the deposition uniformity obtained when the wafer is placed in entrance region of the reactor. This is due to the fact that there is enhanced mass transfer to the wafer surface in a turbulent flow field in comparison to a developing boundary layer flow. Figure 13 shows the comparison between the scaled mass fraction profiles (i.e., ratio of $SiHCl_3$ mass fraction to the inlet $SiHCl_3$ mass fraction) at the center of the wafer when the wafer is placed in a developing turbulent flow and when the wafer is placed in a fully developed turbulent flow. The difference in the boundary layer thickness for the two cases is 0.7 mm. As this difference is not significant, deposition rates are not greatly different. Figure 13 also

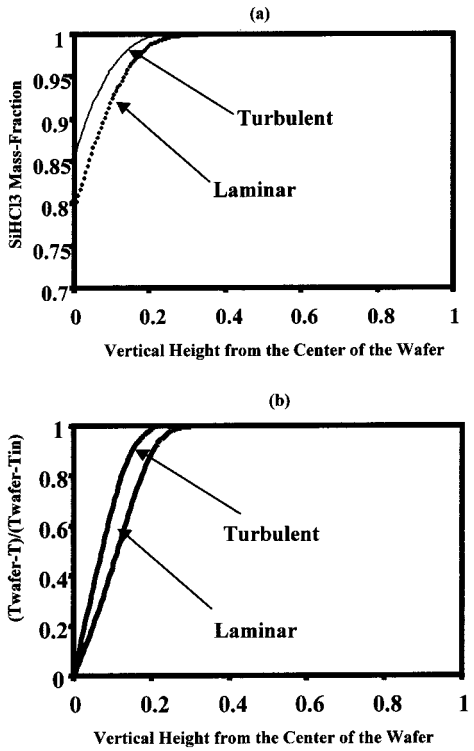

Figure 13. Scaled (a) mass fraction profile of $SiHCl_3$ and (b) temperature profile along the dimensionless reactor height between the center of the wafer and the top reactor wall when the wafer is placed in the developing laminar regime of a turbulent flow and when the wafer is placed in a fully developed turbulent flow. $Re_H = 5000$ ($H = H$), $V_{in} = 30$ m/sec, $T_{wafer} = 1423$ K, and $w_{SiHCl_3,in} = 0.82$.

shows that the temperature boundary layers also become very thin in the high flow rate reactors. Therefore, as mentioned before, in short height and high flow rate reactors, there will not be issues of over heating of the top quartz reactor wall.

Although the fully developed turbulent flow reactor has a superior performance, the expenditure to be borne in an industrial setup for the increased length of the turbulent reactor and the real estate the reactor occupies must be considered when a comparison between the performance of these two reactors is made. As the concern with the fully turbulent reactor is the reactor length required to achieve a fully turbulent flow field, simulations using wire grids at the entrance of the reactors were performed to examine the effect of the grids on the development length. However, it was observed that the turbulence generated by the grids dissipated very rapidly beyond the grids. Hence, the development length was not greatly influence by the presence of the grids.

VII.3. Discussions. A number of issues need to be considered before operating commercial single-wafer CVD reactors at high flow rates, as suggested by our studies. Specifically, the quartz reactor walls should be made thicker to handle the forces due to increasing gas velocity. Clearly, for the type of flow rates that will be needed, there will be convective heat losses at the leading edge of the wafer. However, our simulations clearly show that when the wafer is placed in the inlet region, the convective losses are not very significant. Hence, the SiC ring surrounding the silicon wafer should experience most of the convective losses. Because we are only considering low Reynolds number turbulent

flows, the convective losses are once again not very significant. Therefore, the SiC ring should perform adequately. In case of difficulties with wafer temperature control, a slightly longer SiC ring can be placed around the wafer.

VII. Summary

A three-dimensional simulation model of a horizontal CVD reactor has been used to explore new strategies leading to high production of quality wafers. As the $SiHCl_3-H_2$ system is a widely used precursor for epitaxial silicon deposition in industrial applications, we have chosen to focus our model development on this system. Specifically, we have examined cases where the wafer is placed in the entrance region of a developing turbulent flow and in a fully developed turbulent flow and have shown that combining this strategy with reduction in reactor height allows for high-volume production of quality wafers with minimum material usage. In addition, it has been demonstrated that, for the production of large diameter wafers that operate at low wafer temperatures, a similar strategy can be used.

Acknowledgment

This work has been supported in part by a grant from MEMC Electronic Materials, Inc. We are grateful to Dr. Gregory M. Wilson and Dr. Sriram Ramanathan for helpful comments.

Appendix A

gases	specific heat as a function of temperature (J/(kg K))
hydrogen	$1.408 \times 10^4 + 6.33 \times 10^{-1}T$
trichlorosilane	$5.96 \times 10^2 + 6.76 \times 10^{-2}T$
HCl	$8.09 \times 10^2 - 5.5 \times 10^{-2}T + 7.20 \times 10^{-5}T^2 - 1.34 \times 10^{-8}T^3$

The specific heat of the gas mixture is calculated using the following relationship:

$$C_{p\mathrm{SiHCl_3-H_2}} = w_{\mathrm{SiHCl_3}} C_{p\mathrm{SiHCl_3}} + w_{\mathrm{H_2}} C_{p\mathrm{H_2}} \quad \text{(A.1)}$$

gases	viscosity as a function of temperature (Pa sec)
hydrogen	$3.0 \times 10^{-6} + 2.0 \times 10^{-8}(T/298) - 3.0 \times 10^{-12}(T/298)^2$
trichlorosilane	$2.0 \times 10^{-7} + 4.0 \times 10^{-8}(T/298) - 5 \times 10^{-12}(T/298)^2$
HCl	$4.0 \times 10^{-7} + 5.0 \times 10^{-8}(T/298) - 8.0 \times 10^{-12}(T/298)^2$

The viscosity of the gas mixture is calculated using the following relationship:

$$\mu_{\mathrm{mix}} = \sum_{i=1}^{n} \frac{x_i \mu_i}{\sum_{j=1}^{n} x_j \Phi_{ij}} \quad \text{(A.2)}$$

where

$$\Phi_{ij} = \frac{1}{\sqrt{8}}\left(1 + \frac{\mathrm{M}_i}{\mathrm{M}_j}\right)^{-1/2}\left(1 + \left(\frac{\mu_i}{\mu_j}\right)^{1/2}\left(\frac{\mathrm{M}_j}{\mathrm{M}_i}\right)^{1/4}\right)^2 \quad \text{(A.3)}$$

gases	thermal conductivity as a function of temperature (W/(m K))
hydrogen	$4.7 \times 10^{-2} + 5.0 \times 10^{-4}T - 6.0 \times 10^{-8}T^2$
trichlorosilane	$6.2 \times 10^{-3} + 5.0 \times 10^{-5}T - 7.0 \times 10^{-9}T^2$
HCl	$1.0 \times 10^{-4} + 5.0 \times 10^{-5}T - 3.0 \times 10^{-9}T^2$

The thermal conductivity of the gas mixture is calculated using the following relationship:

$$\lambda = \xi \sum_{i=1}^{n} \lambda_i x_i + (1 - \xi) \sum_{i=1}^{n} \left(\frac{x_i}{\lambda_i}\right)^{-1} \quad \text{(A.4)}$$

where

$$\xi = 0.312 + 0.325 x_{\mathrm{H_2}} - 0.311 x_{\mathrm{H_2}} + 0.469 x_{\mathrm{H_2}} \quad \text{(A.5)}$$

The expressions A.2−A.4 are obtained from Bretsznadjer.[24]

Appendix B

gas pairs	binary diffusion coefficients as a function of temperature (m^2/s)
hydrogen−hydrogen	$4.0 \times 10^{-5}(T/298) + 10^{-4}(T/298)^2 - 8.0 \times 10^{-6}(T/298)^3 + 5.0 \times 10^{-4}(T/298)^4$
trichlorosilane−hydrogen	$7.0 \times 10^{-6}(T/298) + 3.0 \times 10^{-5}(T/298)^2 - 3.0 \times 10^{-6}(T/298)^3 + 2.0 \times 10^{-4}(T/298)^4$
HCl−hydrogen	$2.0 \times 10^{-5}(T/298) + 5.0 \times 10^{-5}(T/298)^2 - 3.0 \times 10^{-6}(T/298)^3 + 7.0 \times 10^{-8}(T/298)^4$

The thermal diffusion coefficients of the gas species are calculated using the following relationships:

$$D^{\mathrm{T}}_{\mathrm{SiHCl_3}} = \frac{P}{MRT} M_{\mathrm{SiHCl_3}} M_{\mathrm{H_2}} D_{\mathrm{SiHCl_3-H_2}} k_{\mathrm{SiHCl_3-H_2}} \quad \text{(A.6)}$$

$$D^{\mathrm{T}}_{\mathrm{HCl}} = \frac{P}{MRT} M_{\mathrm{HCl}} M_{\mathrm{H_2}} D_{\mathrm{HCl-H_2}} k_{\mathrm{HCl-H_2}} \quad \text{(A.7)}$$

where the thermal diffusion ratios ($k_{\mathrm{HCl-H_2}}$ and $k_{\mathrm{SiHCl_3-H_2}}$) are obtained as a function of the gas species concentrations and temperature from Hirshfelder.[25]

Nomenclature

C_{A} = molar concentration of chemical species A (kmol m^{-3})
$C_{p\mathrm{A}}$ = Specific heat of chemical species A (J kg^{-1} K^{-1})
Da = Damkohler number
D_{AB} = binary diffusion coefficient of chemical species A in diluent B (m^2 s^{-1})
$D_{\mathrm{A}}^{\mathrm{T}}$ = thermal diffusion coefficient of chemical species A in diluent B (kg m^{-1} s^{-1})
e_z = unit normal vector along z direction
g = acceleration due to gravity (m s^{-2})
Ga = Gay-Lussac number
Gr = Grashof number
G_{d} = dimensionless silicon deposition rate
G_x = silicon deposition rate at any position x on the wafer surface (microns min^{-1})
h = heat transfer coefficient (W m^{-2} K^{-1})
$j_{\mathrm{A}}^{\mathrm{C}}$ = diffusion flux of chemical species A driven by concentration gradient (kg m^{-2} s^{-1})
$j_{\mathrm{A}}^{\mathrm{T}}$ = diffusion flux of chemical species A driven by temperature gradient (kg m^{-2} s^{-1})
K_{ad} = adsorption rate constant (m s^{-1})
K_{f} = reaction rate constant (m^4 $kmol^{-1}$ s^{-1})
K_{r} = desorption rate constant (m s^{-1})

L = characteristic reactor dimension (m)
MW_A = molecular weight of a gas species A (kg kmol^{-1})
n = unit normal vector
P = pressure (Pa)
Pr = Prandtl number
R = universal gas constant (J kmol^{-1} K^{-1})
$R_{s,A}$ = surface chemical reaction rate of chemical species A (kg m^{-2} s^{-1})
R_{ad} = rate of adsorption (kmol m^{-2} s^{-1})
Re = Reynolds number
Re_H = Reynolds number based on the height of the reactor
Re_x = Reynolds number based on the distance along the mean-flow direction
R_{Si} = silicon deposition rate (kmol m^{-2} s^{-1})
Sc = Schmidt number
T = temperature (K)
Td = thermal diffusion number
T_{Inf} = ambient gas temperature (K)
T_{wafer} = wafer surface temperature (K)
T_{wall} = wall temperature (K)
U = velocity of gas (m s^{-1})
$u^+ = Uu^*$
$u^* = (\tau_{wall}/\nu)^{0.5}$
τ_{wall} = wall shear stress (kg m^{-1} s^{-2})
V = characteristic velocity of gas (m s^{-1})
V_{in} = inlet velocity of the gas (m s^{-1})
w_A = mass fraction of chemical species A
$w_{A,in}$ = mass fraction of chemical species A at the reactor inlets
X = fraction of reactive sites on wafer surface occupied by $SiHCl_3$
$y^+ = yu^*/\nu$
ρ = density of gas (kg m^{-3})
μ = viscosity of gas (kg m^{-1} s^{-1})
ν = kinematic viscosity of gas (m^2 s^{-1})
λ = thermal conductivity of gas (W K^{-1})
$\wedge$ = dimensionless parameter

Literature Cited

(1) Kleijn, C. Transport Phenomena in Chemical Vapor Deposition Reactors. Ph.D. Thesis, Voorburg, The Netherlands, 1991.

(2) Jensen, K. F.; Simka, H.; Mihopoulos, T. G.; Futerko, P.; Hierlemann, M. Modeling approaches for rapid thermal chemical vapor deposition: combining transport phenomena with chemical kinetics. In *Advances in Rapid Thermal and Integrated Processing*; Roozeboom, F., Ed.; Series E-Applied Sciences; Kluwer Academic Publishers: The Netherlands, 1995; Vol. 318, pp 305−331.

(3) Kleijn, C.; Hoogendoorn, C. J. A study of 2-D and 3-D transport phenomena in horizontal chemical vapor deposition reactors. *Chem. Eng. Sci.* **1991**, *46*, 321−334.

(4) Moffat, H. K.; Jensen, K. F. Complex flow phenomena in MOCVD reactors, I: horizontal reactors. *J. Cryst. Growth* **1986**, *77*, 108−119.

(5) Kommu, S.; Wilson, G. M.; Khomami, B. A theoretical/experimental study of silicon epitaxy in horizontal single-wafer chemical vapor deposition reactors. *J. Electrochem. Soc.* **2000**, *147* (4), 1538−1550.

(6) Fotiadis, D. I.; Kieda, S.; Jensen, K. F. Transport phenomena in vertical reactors for metalorganic vapor phase epitaxy: I. Effects of heat transfer characteristics, reactor geometry, and operating conditions. *J. Cryst. Growth* **1990**, *102*, 441−470.

(7) Van de Ven, J.; Rutten, G. J. M.; Raaymakers, M. J.; Giling, L. J. Gas phase depletion and flow dynamics in horizontal MOCVD reactors. *J. Cryst. Growth* **1986**, *76*, 352−372.

(8) Moffat, H. K.; Jensen, K. F. Three-dimensional flow effects in silicon CVD in horizontal reactors. *J. Electrochem. Soc.* **1988**, *135* (2), 459−471.

(9) Coltrin, M. E.; Kee, R. J.; Evans, G. H. A mathematical model of the fluid dynamics and gas-phase chemistry in a rotating disk chemical vapor deposition reactor. *J. Electrochem. Soc.* **1989**, *136* (3), 819−829.

(10) Ouzzani, J.; Chiu, K.; Rosenberger, F. On the 2-D modeling of horizontal CVD reactors and its limitations. *J. Cryst. Growth* **1988**, *91*, 497−508.

(11) Habuka, H.; Katayama, M.; Shimada, M.; Okuyama, K. Numerical evaluation of Silicon-thin film growth from $SiHCl_3$−H_2 gas mixture in a horizontal chemical vapor deposition reactor. *Jpn. J. Appl. Phys., Part 1* **1994**, *33*, 1977−1985.

(12) Habuka, H.; Nagoya, T.; Katayama, M.; Shimada, M.; Okuyama, K. Modeling of epitaxial Silcion thin-film growth on a rotating substrate in a horizontal single-wafer reactor. *J. Electrochem. Soc.* **1995**, *142*, 4272−4278.

(13) Habuka, H.; Nagoya, T.; Mayasumi, M.; Katayama, M.; Shimada, M.; Okuyama, K. Model on transport phenomena and epitaxial growth of silicon thin film in $SiHCl_3$−H_2 system under atmospheric pressure. *J. Cryst. Growth* **1996**, *169*, 61−72.

(14) Ho, P.; Balakrishna, A.; Chacin, M. J.; Thilderkvist, A. Chemical kinetics for modeling Silicon epitaxy from chlorosilanes. In *Fundamental Gas-Phase and Surface Chemistry of Vapor-Phase Materials Synthesis*; Allendorf, M. D., Zachariah, M. R., Mountziaris, L., McDaniel, A. H., Eds.; The Electrochemical Society Proceeding Series; Electrochemical Society: Pennington, NJ, 1998; Vol. 98 (23), pp 117−122.

(15) Roozeboom, F. *Advances in Rapid Thermal and Integrated Processing, 318*; Series E-Applied Sciences; Kluwer Academic Publishers: The Netherlands, 1995.

(16) Santen, H. V.; Klien, C. R.; Van Den Akker, H. E. A. Turbulence and its influence on mass transfer in a rotating disk CVD reactor. *Electrochemical Society Proceedings*; Electrochemical Society: Pennington, NJ, 1987; Vol. 97 (25), pp 214−221.

(17) *DIPPR database*, CFX 4.1c Solver; AEA Technology, CFX International: Oxfordshire, U.K., 1997.

(18) Launder, B. E.; Sharma, B. T. Application of the energy dissipation model of turbulence to the calculation of flow near a spinning disk. *Lett. Heat Mass Transfer* **1974**, *1*, 131−137.

(19) Launder, B. E.; Spalding, D. B. *Lectures in mathematical models of turbulence*; Academic Press: London, U.K., 1972.

(20) *CFX 4.1c Solver*; AEA Technology, CFX International: Oxfordshire, U.K., 1997.

(21) Patankar, S. V. *Numerical Heat Transfer and Fluid Flow*; Hemisphere Publishing Corporation: Bristol, PA, 1983.

(22) Bloem, J. High chemical vapour deposition rates of epitaxial silicon layers. *J. Cryst. Growth* **1973**, *18*, 70−76.

(23) Schlichting, H. *Boundary-Layer Theory*, 7th ed.; McGraw-Hill: New York, 1968.

(24) Bretsznajder, S. *Prediction of Transport and other Physical Properties of Fluids*; Pergamon Press: Oxford, U.K., 1971.

(25) Hirscfelder, J. O.; Curtiss, C. F.; Bird, R. B. *Molecular Theory of Gases and Liquids*; John Wiley and Sons: New York, 1967.

Received for review May 9, 2001
Accepted December 12, 2001

IE010412W